



تأثير الظروف المناخية السائدة في ملوحة التربة في واحة الخارجة اعتمادا على مرئيات القمر الصناعي لاندسات 8 والسلاسل الزمنية المناخية "

د/ وليد عباس
مدرس بقسم الجغرافيا، كلية الآداب
جامعة عين شمس

hosam.ismael@artnv.au.edu.eg

أ.م.د/ حسام إسماعيل
أستاذ مساعد بقسم الجغرافيا، كلية الآداب
جامعة الوادي الجديد

walid.abbas@art.asu.edu.eg

د/ شربات بشندي

مدرس بقسم الجغرافيا، كلية الآداب، جامعة القاهرة

sharabathamdy@yahoo.com

تاريخ استقبال البحث: 2020/7/5

تاريخ قبول النشر: 2020/7/27

المستخلص :

ما لا يمكن إنكاره للظروف المناخية السائدة في مصر والعالم من تأثيرات متسارعة للتغيرات المناخية، وازدياد حدة وسرعة موجات الحر والأحداث المناخية المتطرفة؛ من المتوقع أن ترتفع وتيرة تأثير تلك الأحداث المناخية القاسية الأمر الذي يؤدي إلى تفاقم ظواهرات ومشكلات أهمها الجفاف، وتدهور الأراضي، وموجات الحر، وتملح التربة في المستقبل على الأراضي القاحلة وشبه القاحلة، خاصة في واحة الخارجة، التي تنتمي مناخيا إلى نوع المناخ الصحراوي في الأجزاء الجنوبية من مصر طبقا لتصنيف كوبن (BWh).

إن تملح التربة هو أحد مشاكل تدهور الأراضي الزراعية في واحة الخارجة الأمر الذي يمثل تهديدا مباشرا لتنمية تلك المناطق القاسية مناخيا بسبب آثاره المؤسفة على إنتاجية الأراضي، وقد في كل عام تتدهور العشرات من الأفدنة الزراعية من الأراضي الزراعية بسبب تملح التربة الأولى أو الثانوي، ونتيجة لذلك، أصبحت هذه المشكلة مصدر قلق اقتصادي وبيئي خطير في محافظة الوادي الجديد. وبالتالي فإن رصد مشكلة تملح التربة في واحة الخارجة في منتهى الأهمية لدعم إجراءات اتخاذ القرار لتقليل الآثار السلبية الناتجة عن تدهور الأراضي بسبب التملح باعتبار واحة الخارجة من المناطق الواعدة للتنمية الزراعية في مصر والتي دخلت مؤخرا ضمن مشروع الدولة لزراعة مليون ونصف مليون فدان. ومن الجدير بالذكر أن التقنيات الحديثة القائمة على الاستشعار عن بعد ونظم المعلومات الجغرافية توفر معلومات مكانية فعالة في دراسة الأراضي الزراعية بشكل عام والتربة المملحة بشكل خاص.

هدفت الدراسة الحالية إلى دراسة أثر الظروف المناخية السائدة على كشف ورصد ملوحة التربة بواحة الخارجة باعتبارها من المناطق الواعدة للتنمية المستدامة. ولتحقيق أهداف الدراسة ، استخدمت الدراسة الحالية تقنيات الاستشعار عن بعد ونظم المعلومات الجغرافية ، وقد تم الحصول على عينات من التربة المتملحة في نفس وقت الفصل المناخي (فصل الصيف) للمريثيات الفضائية من القمر الصناعي لاندسات -8 المستوى الأول وذلك خلال يوليو 2018. لم تعتمد الدراسة الحالية على بيانات السلاسل الزمنية وصور الأقمار الصناعية فحسب ، بل استندت أيضاً إلى التحقيقات الميدانية في واحة الخارجة والتحليلات الإحصائية والتحليلات المعملية المتخصصة. وقد تبين من الدراسة أن هناك الكثير من العوامل المسببة لتملح التربة في واحة الخارجة لعل الظروف المناخية أهمها، ومن أهم تلك العوامل الطرق البدائية للري بالغمر، والسياسة الزراعية غير المدروسة.

كما تبين أن حوالي 85% من التربة في واحة الخارجة لها قيم ملوحة تزيد عن 4 dS m⁻¹، ويبدو آثار هذا التملح واضحة في التربة والنباتات. وقد وجد أن مساحة التربة شديدة الملوحة تشغل مساحة 6668 كم² أو حوالي 35.5% من المساحة الإجمالية لواحة الخارجة. كما تبين من خلال دراسة التوزيع المكاني لملوحة التربة أن فئة الملوحة العالية تبلغ حوالي 22.2% ، وتحتل 4733.7 كم² ، وتشمل فئات الملوحة المعتدلة والمنخفضة 24% و 15.3% ، وتغطي حوالي 5462.6 كم² ، 2820 كم² من واحة الخارجة على الترتيب.

الكلمات المفتاحية: الظروف المناخية ، التبخر ، الملوحة ، الاستشعار عن بعد ، الخارجة.

1-Introduction:

In the past decades, climate events have become more abnormal. Such abnormal climate phenomena as severe droughts and unusual storms can result in land degradation and soil salinization (Zhang, L, 2008). However, the processes behind these emerging geo-hazards induced by abnormal climate conditions have not been quite understood. Climate is a considerably compound issue, in order to the earth atmosphere interaction which extremely different over the place, time and eventually inspire a special type of climate at a specific location (Hossam Ismael, 2015). It has been recognized as a soil forming factor for many years. Furthermore, the climate is the most significant factor affecting the soil, its development and its problems, specifically in hyper dry lands such Kharga Oasis in the Western Desert of Egypt. Among the significant consequences resulting from prevailing climate conditions in arid and semiarid lands, ranks soil salinity and land degradation.

Soil salinity is a major concern in the arid and semi-arid regions of the world and considered an environmental menace (Metternich and Zinck, 2003; Shrestha et al, 2005b; Kumar et al., 2018; Abdelgadir et al, 2019). It had become a major environmental issue. Nearly, 800 million hectares of land worldwide, more than 6 % of the overall surface area is affected by salinization processes (Rattan Lal et al, 2014). Moreover, climate change is exacerbating the deterioration of arable land in arid and semi-arid regions. Especially over dry land areas, soil salinization is more likely to occur because of harsh climatic conditions and irrational irrigation practices (Fan, X et al., 2016).

Albeit, Salinization is a subtle natural hazard that results from lower levels of precipitations than what is considered normal. It must be considered a relative rather than an absolute condition. Soil Salinization is local in extent and each region has specific climatic characteristics. This phenomenon is progressing rapidly in the world and concerns a fifth of irrigated land (Kallel, A et al, 2017).

The present study tried to discuss the prevailing climate conditions on soil salinity of Kharga Oasis in Egypt based to Köppen's climatic classification along with the spatial and inter-seasonal variations of air temperature and soil temperature. In this paper, analyses on the soil salinity caused by prevailing climatic conditions are studied by means of studying, detecting and monitoring soil salinity of Kharga Oasis based on Landsat 8 OLI satellite and climate time series.

Increasing the number of studies on identifying and monitoring soil salinity indicates the prevailing benefit in conserving soil productivity and mitigating the negative effects of salinization. The efficiency of using satellite images data and GIS for monitoring soil salinity has been set in several previous studies to be the most resourceful. Specific findings including experienced and new mapping techniques, sensing techniques, satellite data, and figure out of salinity for each case study are summarized in (Table 1).

The modern generation of polar-orbiting sun-synchronous multispectral RS data has newly become applicable. Multispectral sensors such as Landsat, SPOT, ASTER, IKONOS, MODIS, and IRS series have provided many opportunities of monitoring and mapping soil salinity since 1990 (Allbed and Kumar, 2014). Landsat 8 Operational Land Imager (OLI) has been widely used for an improved global environment and security monitoring at the medium resolution (30 m), especially for soil salinity assessment (Tran et al., 2019; Wulder et al., 2019).

The essential objectives of the present study are to Detecting soil salinity in Kharga Oasis using Landsat 8 OLI satellite and time-series data (1940-2018), analyze the effectiveness of using regression analysis between spectral information and salinity values to model the extent of soil salinization along with Kharga Oasis in the Western Desert of Egypt as one of the promising regions for agricultural development in the country. To achieve that objective, soil salinity indices were applied to the Landsat 8 (OLI) data with truth ground data measurements to validate the percentage of prediction accuracy based on different error assessment path.

Finally, temporal variations in soil salinity and the motivating forces behind were determined based on the retrievals. The limitation to this methodology is the spatial resolution of the Landsat-8 OLI (30 m) and the fundamental difficulty in detecting low levels of surface soil salinity, however, this study examines the suitability of multiple spectral bands in detecting salinity in a regional basis. The aim of the current study was to assess the level of salinity in Kharga oasis through the application of salt indices and developing different salinity mapping by using a satellite image from the Landsat-8 Operational Land Imager (OLI) during July 2018.

(Table 1) The recent studies preferred to utilize RS technology in comparison to other tools for monitoring soil salinity within 2015-2018

| Published Year | Study Area | Climate Regime | Satellite Data | Analysis/ Mapping Methods | Reason of salinity | Reference |
|----------------|----------------------|------------------------|------------------------------------|---|---|---------------------|
| 2018 | Junggar Basin, China | Bsk (Cold Arid Steppe) | MODIS | Empirical model decomposition method, linear and Random Forest (RF) regression models | Disturbance in soil~ water balance due to environmental factors | (Ma & Yang, 2018) |
| 2018 | North west China | BWk (Cold Arid Desert) | Landsat OLI, Huanjing (HJ) 1-B CCD | Develop optimal band Difference Index (DI), Ratio Index (RI), and Normalization Index (NDI) algorithms, Bootstrap-BP neural network model | Rare precipitation and high evaporation | (Wang et al., 2018) |
| 2018 | Pomp | Cfb | Landsat | Regression analysis and ordinary | Parent | (Caster |

| | | | | | | |
|------|-----------------------|------------------------|-----------------------------|---|---|-------------------------------|
| | enillo, Grañén, Spain | | t 5 TM | kriging (OK) | material | ad, 2018) |
| 2017 | South Khorasan, Iran | BWh (Hot Arid Desert) | Landsat ETM+ | Interpretation and calculation of salinity index from satellite data (Normalized Difference Salinity Index- NDSI) Regression analysis | Region retains water and allows no outflow due to its geologic properties | (Saghafi, 2017) |
| 2017 | Turkey | BSk (Cold Arid Steppe) | Landsat 5 TM, Landsat 8 | Utilizing salinity indices, linear regression analysis | Saline lake | (Gorji et al., 2017a) |
| 2017 | South Africa | BSh (Hot Arid Steppe) | Aerial photography | Principal component analysis (PCA) Regression modeling, Kriging | Insufficient natural drainage | (Vermeulen and Niekerk, 2017) |
| 2016 | West Bengal, India | Aw | Landsat MSS, TM and ETM+ | Kriging, utilizing indices (NDVI, SAVI, NDSI) | Seawater and wind impacts | (Das et al., 2016) |
| 2016 | Morocco | BSh (Hot Arid Steppe) | Landsat 5 TM, Landsat 8 OLI | Utilizing the Soil Salinity Spectral Indices (SSSI)-(OLI-SI index, NDVI), simple linear regression between sampled soil EC | Poor irrigation and agricultural practices, climate change effect | (El et al., 2016) |
| 2016 | Çukurova, Turkey | Csa | Landsat TM, ETM | Object based classification, vegetation indices (NDVI, NDWI, SAVI, GVI, PVI, WDI, WETNESS), multi-linear regression (MLR) and SLR, radial | Inappropriate irrigation practices, high groundwater | (Satir and Berberoglu, 2016) |

| | | | | | | |
|------|-------------------------------|-----------------------|-------------------------|---|---|----------------------------|
| | | | | basis function technique | table nearby the sea | |
| 2016 | Western Desert, Egypt | BWh (Hot Arid Desert) | Landsat 8 OLI | Regression analysis, utilizing satellite image (SAVI algorithm) | High evapotranspiration rates, Low precipitation | (Hereher and Ismael, 2016) |
| 2015 | Algeria | Csa | Landsat ETM+ | Multiple linear regression model | Extensive agricultural practices | (Yahiaoui et al., 2015) |
| 2015 | East Nile Delta Region, Egypt | BWh (Hot Arid Desert) | Landsat 8, ASTER, GDEM | Principal component analysis, utilizing salinity indices | Poor quality groundwater, inappropriate irrigation and anthropogenic activities | (Arnouts et al., 2015) |
| 2015 | Brazil | BSh (Hot Arid Steppe) | OLI/Landsat-8, Hyperion | Principal component analysis (PCA), support vector machine (SVM), regression analysis | High evapotranspiration, low precipitation | (Moreira et al., 2015) |

2. Materials and methodology:

2-1. Study area:

Kharga is one of seven separate Oases circulated within the Western Desert of Egypt at about 230 km west of the Nile and about 650 km southwest of Cairo (Fig. 1). Kharga Oasis experiences the hot desert climate (BWh) according to Koeppen's classification. It belongs administratively to the New Valley Governorate (Hossam Ismael, 2015).

It is located in the southern part of the Egyptian western desert, between longitudes 30°27'00" N - 30°47'00" E, and between latitudes 22°30'14" - 26°00'00" N. The territory of Kharga depression covers about 7500 square kilometers (Ibid, 2015) (Figure. 1).

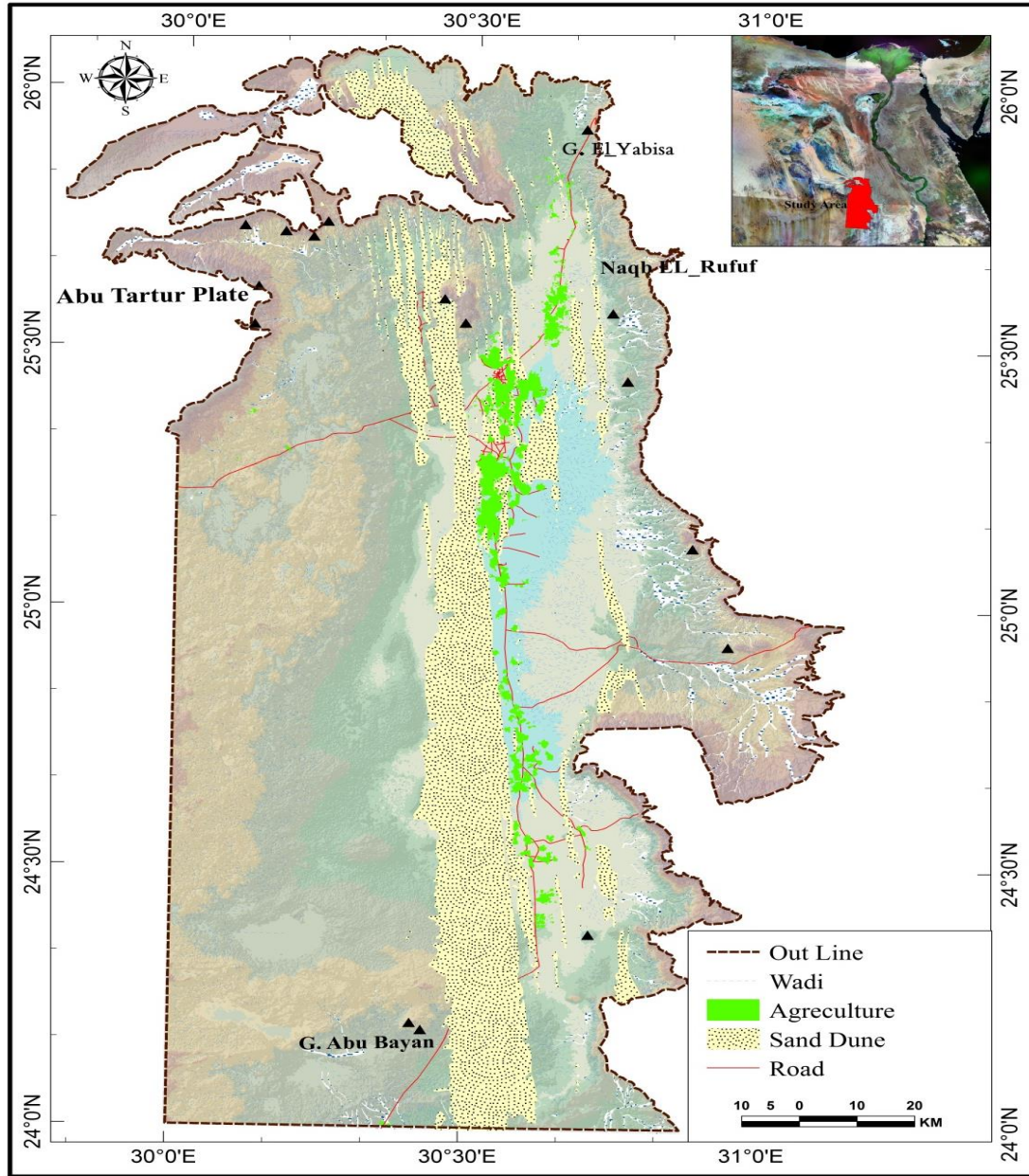


(Figure.1) Delimitation of 'Kharga Oasis

Kharga oasis is extremely hyper arid as it is a part of the dry desert, where descending air moving from the equatorial region produces a strong air mass known as the tropical continental region. Wind basically blows from the north-northwest causing sand dunes to drift, which is a popular issue encroaching upon settlements, farmlands, and roads. Evidently, the region is the driest on the earth's surface, where the incident solar radiation is capable of evaporating over 200 times the amount of precipitation (Ismael, H., 2016).

The air temperatures range from 44°C in summer to 25°C in the winter and potential evapotranspiration is as high as 5 mm/d. Annual precipitation normal does not exceed 2 mm and the rainy days are 0.8 / year. The annual rainfall in most parts of less than 10 mm. According to the aridity index P/ETP ($P =$

precipitation and ETP = potential evapotranspiration, calculated by Penman's formula), the arid regions are classified to hyper-arid ($P/ETP < 0.03$) and arid ($P/ETP = 0.03 - 0.20$) (Mostafa El Gamal, 2012).

Ikonos satellite imagery was used to determine the geographical units affecting soil salinity in Kharga Oasis (Table.2). There is a heavy sand dune field, the great sand sea, occurring north of Kharga and extends until Siwa oasis in the north. Dunes enter the oasis by descending through the northern escarpment particularly from the western side of the plateau (Figure.2). Rates of dune advance have been documented around 6 m/year (Ghadiry et al., 2012).

(Table.2) The geographical units and its represented area in Kharga Oasis by km^2

| No | Geographical units | Area Km^2 | % |
|--------------|--------------------------------------|-------------|------|
| 1 | Rocky Lands Unit | 1766.8 | 9.4 |
| 2 | Foot Hills Unit | 1937.4 | 10.4 |
| 3 | Hills& Mountains | 148.3 | 0.8 |
| 4 | Low Slope | 1548.5 | 8.2 |
| 5 | Gravelly Plains Unit | 382.5 | 2 |
| 6 | Undulating Plains Unit | 4804.4 | 25.5 |
| 7 | Plains covered with thin sand sheets | 734.9 | 3.9 |
| 8 | Semi_ Flat Plains Unit | 1495.2 | 7.9 |
| 9 | High Terraces Unit | 862.8 | 4.6 |
| 10 | Valley Deposit Unit | 402.8 | 2.1 |
| 11 | Decantation Basins Unit | 756.7 | 4 |
| 12 | Sand Dune Unit | 2414.7 | 12.8 |
| 13 | Sand sheets Unit | 625.7 | 3.4 |
| 14 | Nabkhas Units | 111.5 | 0.6 |
| 15 | Playa Unit | 483.6 | 2.6 |
| 16 | Sabkhas Unit | 20 | 0.1 |
| 17 | Agriculture & Urban | 318 | 1.7 |
| Total | | 18813.8 | 100 |

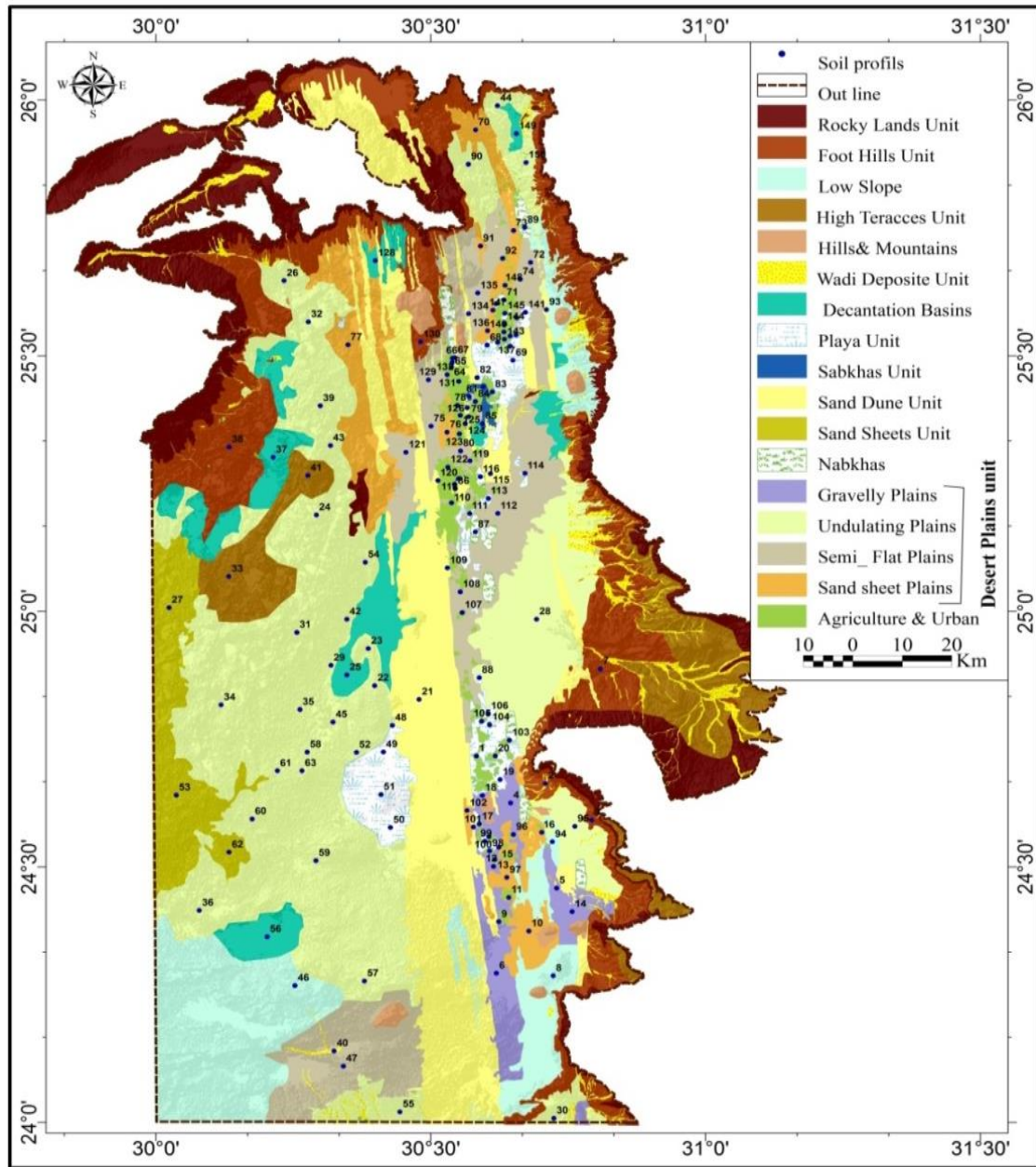


(Figure.2) The soil profile and geographical units in Kharga Oasis

2.2. Climate data.

All climate data utilized in this study are illustrated by original data, corresponding to unpublished data from the Egyptian Meteorological Authority ([www. http://ema.gov.eg](http://ema.gov.eg)) to Kharga station from 1940 to 2018. The climatic data included a solar irradiance, average monthly temperature, average monthly and annual records of rainfall.

The time-series included records of varying temporal length and consisted of data gaps less than 10% data. The series were administered to quality control and homogenization.

2.3. Satellite data Processing procedure.

To accomplish the regression relationship between soil salinity and spectral information, one satellite image from the Landsat-8 OLI satellite image Level 1T product with radiometrically corrected and co-registered to a cartographic projection and terrain corrections was provided by the USGS Earth Explorer gateway (<http://earthexplorer.usgs.gov/>). The image was acquired on July 05, 2018.

The images (path 176, row 42) and (path 176, row 43) have 28.5 m spatial resolution and 11 spectral bands including visible (4 bands), NIR (1 band), SWIR (2 bands) and TIR (2 bands) channels of the spectrum in the Universal Transverse Mercator (UTM) projection. Another digital elevation model (DEM) from the Shuttle Radar Topography Mission (SRTM) was taken for the region in order to feature topographic change along the Oasis with regard to surrounding desert landforms. The DEM is a single band image with a 90 m spatial resolution and 1 m vertical resolution in the UTM projection (Liping Yang et al, 2011).

2.4. Methodology used:

After data acquisition (satellite images and salinity measurements), the research involved: 1- image processing for land cover mapping of cultivated lands and topography analysis, 2- model generation that best fits for salinity correlation, and 3- final image classification for salt-affected soils. ERDAS Imagine 9.4 and ESRI ArcGIS 10.5 Software packages were used to perform image processing and regression relationships. The research design significantly depends upon the spectral behavior and discrepancy between cultivated lands and salt-affected soil (Mohamed E. Hereher and Hossam Ismael, 2016).

The spectral signature detected for pair land cover reveals an apparent distinction in the visible and infrared ratio of the electromagnetic spectrum. Green vegetation considerably absorbs red light at the time where salt-affected soils reflect as much as 50% of the light. On the other hand, although the NIR is reflected equally from both two land features, the light is reflected much greater in the SWIR bands from salt-affected soils than from green vegetation. Applying

spectral indices that use two bands could, thus, be effective to discriminate each of these landforms individually

Although there are 11 spectral bands in the OLI image, six bands have been selected and stacked together to form a new image for the consequent spectral analysis in the Specified ranges of bands: B1 (blue), B2 (green), B3 (red), B4 (NIR), B5 (SWIR1) and B6 (SWIR2). SWIR1 and SWIR2 bands have a wavelength of 1.560 - 1.660 μm and 2.100 - 2.300 μm , respectively (Ibid, 2016). The extent of cultivated lands has been estimated by applying the famous normalized difference vegetation index (NDVI), which is very sensitive to green chlorophyll and consequently could distinguish green vegetation effectively from non-vegetated landforms (Poenaru, V e al, 2015).

The NDVI was appealed to the Landsat-8 OLI image in order to quantify the areal extent of cultivated lands in 2018. As green vegetation highly correlates with NDVI than other non-vegetated features, it was important to highlight the NDVI threshold beyond which all the pixels should be counted as agricultural land.

Regression relationships were supposed to reveal different correlations with soil salinity. The highest R^2 statistics from the abovementioned indices were used to prepare a final salt-affected soil map of Kharga Oasis. The Spatial Modeler in ERDAS Imagine was operated to perform the model and to produce a thematic map of salinity distribution as it provides a value of EC for each pixel in the study area. Soil salinity map was classified in ArcMap Software into five EC classes: < 2 dS/m, 2-4 dS/m, 4-8 dS/m, 8-16 dS/m, and >16 dS/m (Mohamed E. Hereher and Hossam Ismael, 2016).

The DEM was operated to perform a painted relief map, which was classified into four elevation unites as < 150 m; 150-300; 300-450 and 450 m < in ArcMap 10.5. The Landsat-8 OLI image was processed for geometric correction using image to image rectification procedures through a first-order polynomial transform algorithm. The atmospheric correction was carried out by applying the COST Model in ERDAS Imagine depending on the dark-object subtraction method proposed by Chavez (1996) (Ibid, 2016).

3-Results:

The linear regression modeling was applied to tests the numerical relation between the calculated soil EC and the spectral bands in Landsat-8 OLI. Table.3 illustrates the numerical expected models between nine salinity ratios based on Landsat8-OLI, and the soil samples tested EC salinity values at the same time. The SI1 and SI8 models outperformed all other salinity indices

models and demonstrated the highest R-square (0.99), (0.95) relationship between the EC salinity measures respectively.

Table. 3 Results of a linear regression analysis of the nine indexes used to estimate soil salinity values in Kharga Oasis

| Salinity index | Index range | Samples numbers | R ² |
|----------------------------|-------------|-----------------|----------------|
| SI1 (Khan et al, 2005) | 0.7-0.5 | 25 | 0.99 |
| SI2 (Douaoui et al, 2006) | 0.6-0.5 | 25 | 0.82 |
| SI3 (Douaoui et al, 2006) | 1.8-2.4 | 25 | 0.37 |
| SI4 (Gorji, 2016) | 1.4-1.9 | 25 | 0.72 |
| SI5 (Elhag, 2016) | 0.4-2 | 25 | 0.64 |
| SI6 (Dehni & Lounis, 2012) | -0.4-0.3 | 25 | 0.17 |
| SI7 (Mousavi et al.2017) | 0.03-0.8 | 25 | 0.64 |
| SI8 (Elhag, 2016) | 0.06-0.5 | 25 | 0.91 |
| SI9 (Elhag, 2016) | 0.1-1 | 25 | 0.63 |

In general, it was found that the correlations between the spectral bands used to extract the salinity ratio range from the very strong correlation to the relatively low correlation. As shown in Table. 4 The statistical exponential relationships were developed between the spectral bands in Landsat-8 OLI to measure the soil salinity. Table.4 shows that the third spectral band correlates directly and strongly with the fourth, fifth, sixth, and seventh spectral bands, with a correlation value (0.97, 0.06, 0.89, 0.89) respectively.

The fourth spectral band was associated with a very strong direct relationship with the fifth, sixth, and seventh spectral bands, where the value of the relationships are (0.88, 0.94, 0.94), respectively. The fifth spectral band was associated with a strong direct relationship with the sixth and seventh spectral bands, with a value of (0.88, 83) respectively, while it was associated with a relatively low relationship with the second spectral band, where the value of the correlation was 0.73.

Evidently, the correlation value between the sixth and the specter ranges was 0.98, which is a very strong relationship. The sixth spectral band was also associated with a strong correlation with the third, fourth and fifth spectral bands, while it was associated with a relatively low relationship with the third band as it reached 0.7

Table. 4 The correlation matrix to the spectral bans in Landsat-8 OLI

| Correlation matrix | Band 2 | Band 3 | Band 4 | Band 5 | Band 6 | Band 7 |
|--------------------|--------|--------|--------|--------|--------|--------|
| Band 2 | 1 | | | | | |
| Band 3 | 0.95 | 1 | | | | |
| Band 4 | 0.83 | 0.97 | 1 | | | |
| Band 5 | 0.73 | 0.86 | 0.88 | 1 | | |
| Band 6 | 0.70 | 0.89 | 0.94 | 0.88 | 1 | |
| Band 7 | 0.71 | 0.89 | 0.94 | 0.83 | 0.98 | 1 |

DEM reveals that Kharga Oasis is formed mainly of three discontinuous hollows within a plateau terrain (Figure.3): the eastern or Moneira village, the middle or Al-Zayan plain, which is the greatest, and the western or El-Sherka plain. The three hollows take place at a level below 150 m from the mean sea level and cover an area of 2060 km². The deepest point in the Oasis takes place at 18 meters above the mean sea level in the middle hollow (El Sheikh shallow lake), where an artificial lake, Lake El Sheikh, was set up from rural drainage. The northern and eastern escarpments take place at higher than 390 meter above the mean sea level and the southern edge of the Oasis is a plateau desert that reaches up to 290 meters above sea level. Cultivated lands are constricted to these three hollows, where most of the vegetation arises in the middle part.

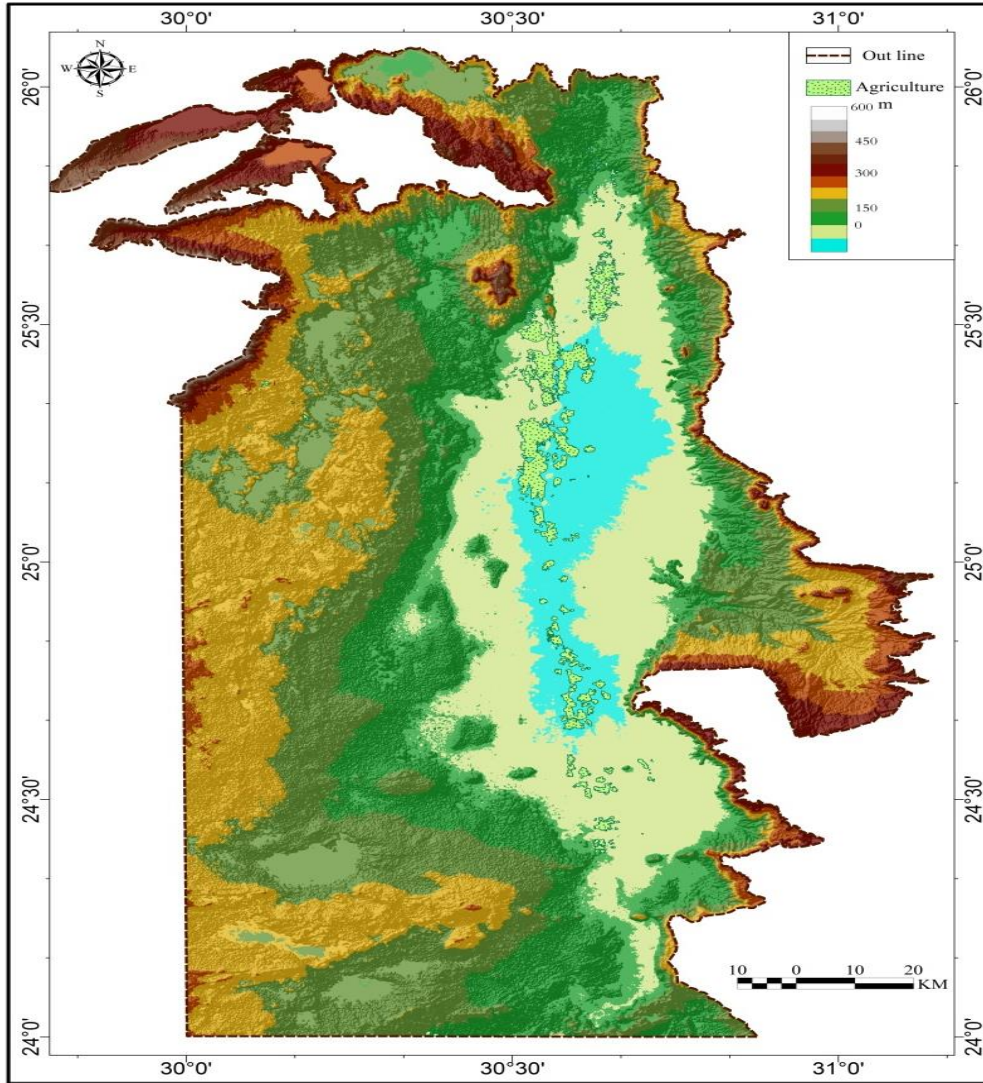


(Figure.3) digital elevation model of Kharga Oasis (SRTM30m)

NDVI threshold value is 0.1; all pixels corresponding or higher than 0.1 are gathered and weighed as agricultural areas. The overall area of agricultural lands as for August 2018 is determined at 604 km² (116,350 acres), represent 32% of the entire Oasis area. The majority of the agricultural lands take place within the intermediate part of the Oasis. Typical desert vegetation is cultivated in the Oasis, usually date palms. Seventeen models reveal positive regression interrelationships and the alternative two (B3/B5 and B4/B3) yield negative interactions (Table.5). The lowest regression coefficient (R^2) is detected for B6/B3 ratio ($R^2 = 0.0689$), while the highest regression coefficient (R^2) is performed for the edged cap (TC) brightness transformation ($R^2 = 0.4395$).

(Table.5): Regression Coefficient models produced to correlate salinity with OLI pixel values

| Spectral | Regression | Regression |
|----------|------------|------------|
|----------|------------|------------|

| band/algebra | Model | Coefficient, R ² |
|-----------------|-------------------------|-----------------------------|
| B1 (Blue) | $y = 46.801x + 11079$ | $R^2 = 0.2271$ |
| B2 (Green) | $y = 88.134x + 11097$ | $R^2 = 0.3435$ |
| B3 (Red) | $y = 142.19x + 11785$ | $R^2 = 0.3923$ |
| B4 (NIR) | $y = 85.674x + 19357$ | $R^2 = 0.3402$ |
| B5 (SWIR1) | $y = 216.63x + 15740$ | $R^2 = 0.3727$ |
| B6 (SWIR2) | $y = 214.2x + 11394$ | $R^2 = 0.3858$ |
| B3/B4 | $y = 0.0034x + 0.6284$ | $R^2 = 0.2367$ |
| B3/B5 | $y = -0.0015x + 0.7862$ | $R^2 = 0.0462$ |
| B3/B6 | $y = -0.0042x + 1.0691$ | $R^2 = 0.1375$ |
| B4/B3 | $y = -0.0066x + 1.5995$ | $R^2 = 0.2385$ |
| B5/B3 | $y = 0.0019x + 1.3271$ | $R^2 = 0.0174$ |
| B6/B3 | $y = 0.0038x + 0.9885$ | $R^2 = 0.0722$ |
| B1*B3 | $y = 2.6298x + 124.85$ | $R^2 = 0.3474$ |
| B3*B4 | $y = 4.832x + 211$ | $R^2 = 0.4179$ |
| B3*B6 | $y = 6.4076x + 105.41$ | $R^2 = 0.4286$ |
| (B6-B1)/(B6+B1) | $y = 0.0042x + 0.0296$ | $R^2 = 0.3729$ |
| (B5-B3)/(B5+B3) | $y = 0.0011x + 0.0397$ | $R^2 = 0.3385$ |
| TC_Brightness | $y = 245.57x + 31855$ | $R^2 = 0.4395$ |

Accordingly, the TC design is employed to provide the salinity map of Kharga Oasis; the tested equation is $y = 245.57x + 31855$, where x is the estimated soil salinity of each pixel in dS/m and y is the value of that pixel in the TC model (the brightness component). The salinity map developed from the represent is illustrated in (Table.7) and (Figure.8) corresponding to IDW interpolation. The total area of bare and fallow soils is 18813.7 km² (100% of kharga oasis).

The majority of these soils (85%) have salinity levels of higher than 4 dS/m. Soils having salinity levels of 4-8 dS/m account for 5462.6 km², those involving salinity levels of 8-16 dS/m are distributed along 4733.7 km², the rest area having salinity levels higher than 16 dS/m account of 6668 km². The majority of salt-affected soils occur within the middle hollow. As for the residual land space of the Oasis, 594 km² (3.3% of the Oasis) is a sandy topography caped by moved sand dunes, sand sheets and shallow lakes from cultivated drainage (Table.6).

(Table.6) Spatial interpolation of soil salinity in Kharga Oasis using GIS

| Soil salinity dS/m | IDW | | Spline | | Kriging | | RBF | |
|-----------------------------|-----------------|------|-----------------|------|-----------------|------|-----------------|------|
| | Km ² | % |
| Non-saline 0-2 | 594 | 3.3 | 6420.9 | 34.1 | 4751.9 | 25.3 | 3912.6 | 20.8 |
| Slightly saline 2-4 | 2255.3 | 12 | 1749.1 | 9.3 | 4300.5 | 22.8 | 2785.4 | 14.8 |
| Moderately saline 4-8 | 5462.6 | 24 | 3277.8 | 17.4 | 5180 | 27.5 | 4028.4 | 21.4 |
| Highly saline 8-16 | 4733.7 | 25.2 | 2072.3 | 11 | 3224.9 | 17.5 | 2451.7 | 13 |
| Extremely saline > 16 | 6668 | 35.5 | 5293.5 | 28.5 | 1356.6 | 7.2 | 5635.7 | 30 |
| Total | 18813. 7 | 100 | 18813. 7 | 100 | 18813.7 | 100 | 18813.7 | 100 |

Spatial interpolation is a fundamental feature of many GIS. It is a method for predicting values of a variable at locations that have not been examined. Maps with isolines or color-smoothed images are usually the visual output of such a process and the maps play a crucial role in decision- making.

However, an interpretation of the basic assumptions and methods applied is a key to the spatial interpolation process. And geostatistics gives the formal mathematical support for such a task (M.M. Jordan et al, 2004).

In this study, we focused on the spatial modeling of EC, extractable sodium, and electrical conductivity. These variables are connected to soil salinity and their spatial estimation and forecast are of essential experimental concern for input to further cultivated or natural schemes. The geostatistical plan for our task is outlined below, followed by the real data interpretation cited as a case study (Table.8).

Alizade Govarchin Ghale, et al (2017) pointed out that many salinity indexes are offered for Landsat images to determine the interpolation of salt-affected soils such (Goossenes and Vanranst, 1996; Al-Khaier, 2003; Abbas and Khan, 2007; Abdul-Qadir and Benni, 2010; Abbas et al., 2013; Allbed and Kumar, 2013; Ahmed and Al-Khafaji, 2014; Arnous and Green, 2015), and among these the most widely used approaches to monitor soil salinity changes using remote sensing data is IDW (figure.4).

The majority of these soils (85%) have salinity levels of higher than 4 dS/m . Soils having salinity levels of 4-8 dS/m account for 5462.6 km², those having salinity levels of 8-16 dS/m are distributed along 4733.7 km², the rest area having salinity levels higher than 16 dS/m account of 6668 km². White salt crusts have been recognized apparently in areas were just left between cultivation that means that the hostile climatic conditions in terms of high temperatures and excessive evaporation are the driving forces for this brilliant desertification. The influence of this serious salinization includes the devastation of soil natural properties and even mortality of domestic vegetation, e.g. date palms.

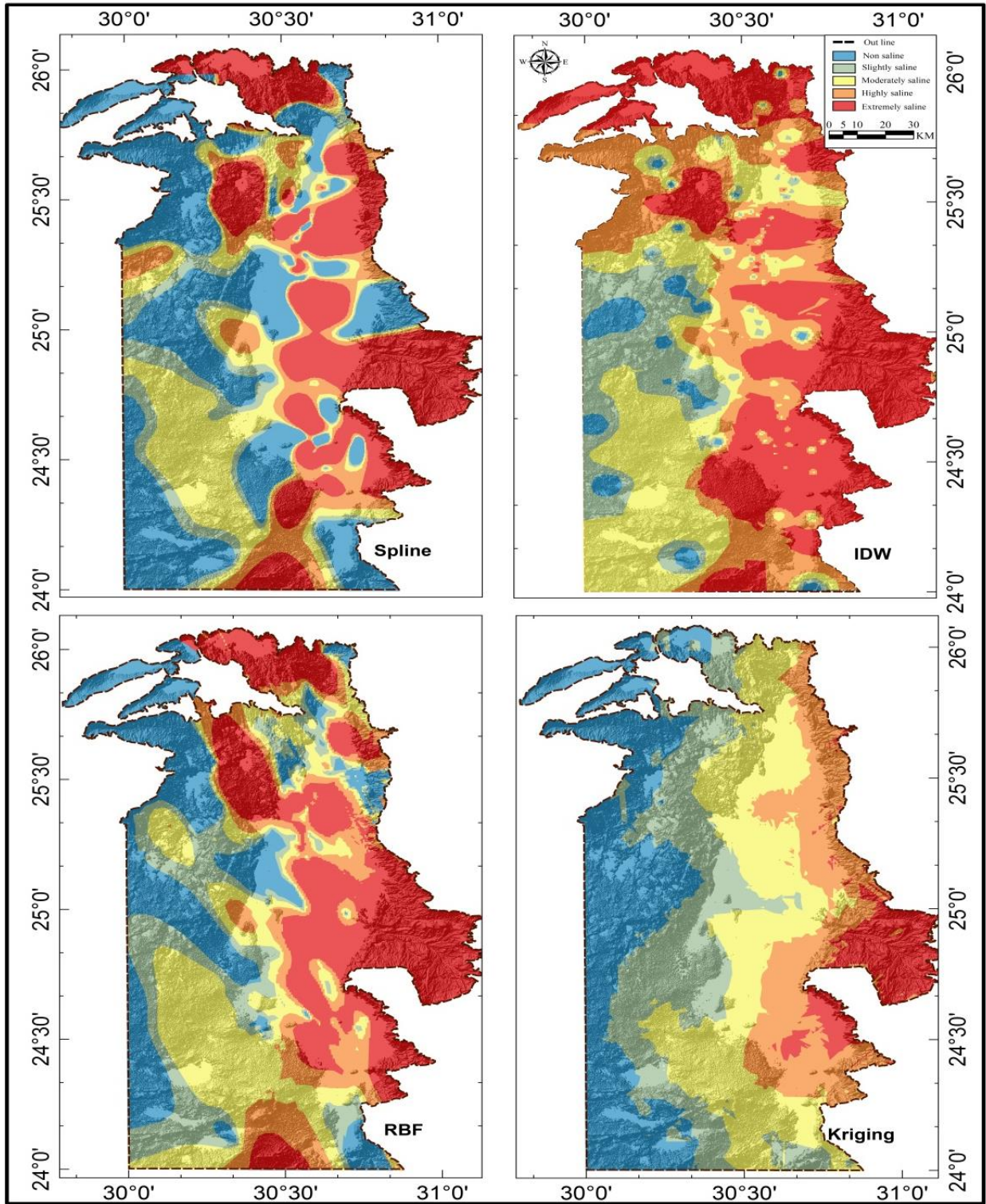


(Figure.4) Spatial interpolation of soil salinity in Kharga Oasis using GIS

4. Discussion:

The results of this study have been indicated that the Landsat 8 satellite images have the possible to outline the regional dissemination of soil salinity to Kharga oasis. The opportunity of eleven several spectral bands in the visible and infrared spectra could use to identify spectral signature of salt-affected soils from other land covers. These eleven spectral bands in the OLI satellite images visualized high interconnection with soil salinity, particularly the red and the SWIR bands.

In Kharga oasis where typical desert vegetation, date palms are grown, there is a likelihood for the occurrence of substantial land areas between palm trees as bare and hence, are prone to salinization and initiation of salt crusts. These crusts are exposed to be remotely sensed from space, the case which is diagnosed by the present study.

The occurrence of the Oasis above this water aquifer makes a water table close to the surface, hence triggering salinization. Because it is one of the most promising areas, it is expected that the Kharga Oasis will accommodate about 1,000,000 persons, which could impact the non-renewable water supply. Water needs for agriculture could not be secured, which would negatively influence soil degradation as water requirements for leaching salts from the soil are not sufficient. Soil salinization is not only the environmental hazard induced by climate conditions dominating Kharga region, sand encroachment is another potential threat to farmlands, settlements, and infrastructure (Figure.5).

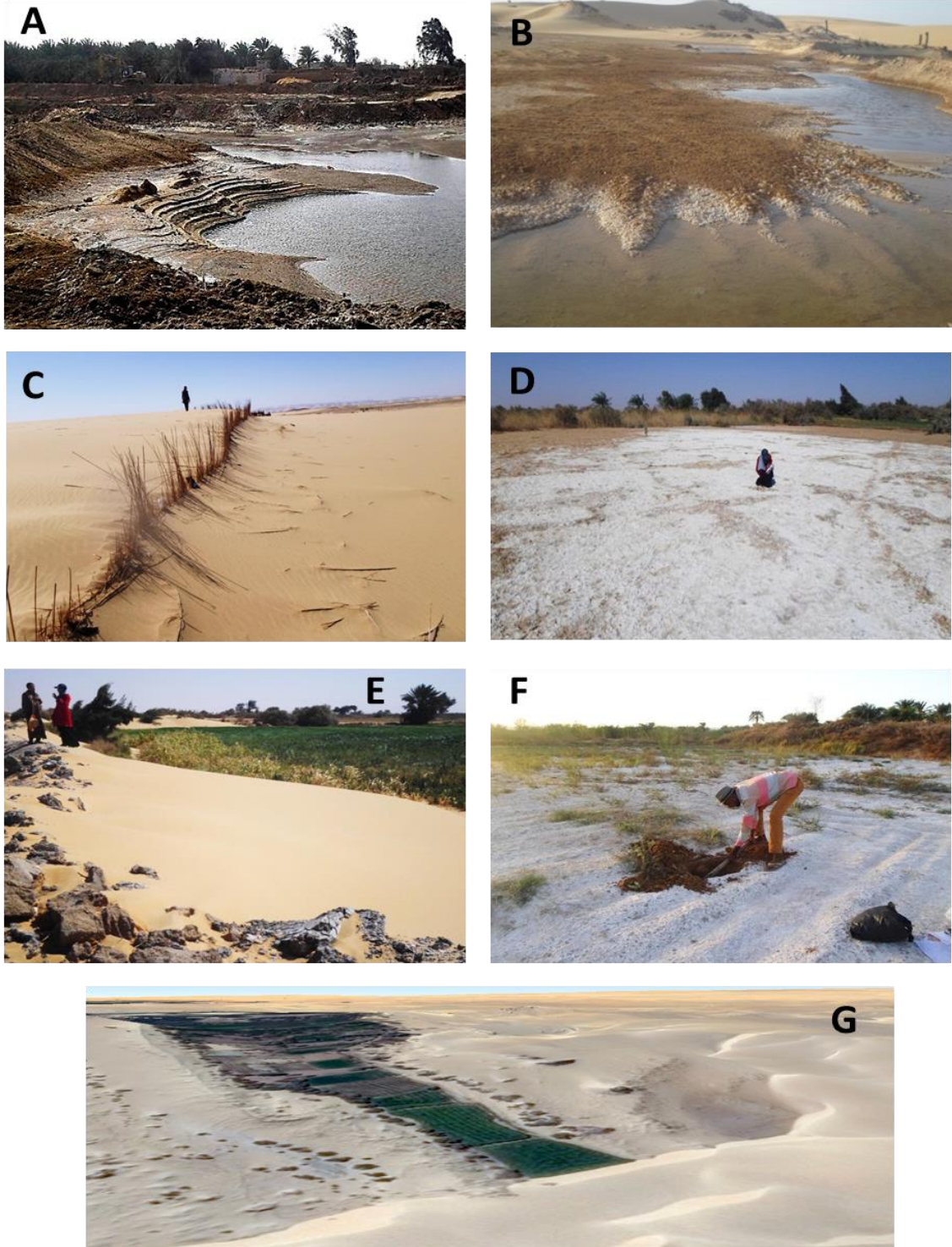


(Figure.5) Ground pictures of Kharga Oasis; a) and b) It turns out that the high level of the groundwater greatly affects the agriculture with excessive salinity, c) and e) the encroachment of sand dunes upon cultivated field, d) the accumulation of salts by evaporation of water from a drainage canal, f) a salt crust at a barren soil area, and g) the dunes threat to agricultural land from digital globe, Google Earth Pro 5 July 2018.

The current study reached these results based on an analysis of climatic elements during the period (1940 - 2018). To illustrate this further, the soils in Kharga Oasis exposed and subjected to direct solar radiation, variation, changes in air temperatures and relative humidity, where air temperature reaches up to 47°C during days' time of summer months (June–July -August) and hauls down to about 14°C during nights time during the same months and varies from less than 5°C during nights time during the winter months (December-January-February). The relative humidity varies from about 57 % during nights time during the winter months (December-January-February) and hauls down to less than 20 % during days' time of the same months and varies from about 52 % during nights time during the summer months (December-January-February) and hauls down to less than 14 % during days' time of the same months in Kharga station (Table. 7).

(Table.7) the normal values of climate elements and its corresponding anomalies during the three distinguished periods (1940-1965, 1965-1990 and 1990-2018) at Kharga station.

| Elements | Normal 1940- 2018 | Anomalies | | |
|-------------------------------|-------------------------|-----------|-----------|-----------|
| | | 1940-1965 | 1965-1990 | 1990-2018 |
| Mean temperature (°C) | 25.4 | -0.85 | +0.3 | + 0.4 |
| Minimum temperature (°C) | 12 | -1.20 | - 0.80 | - 0.75 |
| Maximum temperature (°C) | 41 | + 0.9 | +1.45 | +1.20 |
| Max Absolute temperature (°C) | 52 | - | - | - |
| Min Absolute temperature (°C) | 2 | - | - | - |
| Rainfall amount (mm) | 10.2 | -1.4 | -1.2 | -.08 |
| Sunshine duration (%) | 88.4 | + 1.09 | + 1.02 | +1.1 |
| Wind speed (kt) | 8.6 | + 0.25 | + 0.30 | + 0.35 |
| Evaporation (mm per day) | 12.3 | +0.04 | + 0.08 | +0.1 |

| | | | | |
|------------------------------|------|--------|--------|--------|
| Relative humidity (%) | 57 | + 2.30 | +2.0 | + 2.45 |
| Cloud amount (oktas) | 1.70 | + 0.25 | + 0.45 | +0.5 |

Egyptian meteorological authority, unpublished data

The solar radiation reaches Kharga Oasis lowest intensity in the winter. The rate increases gradually about (18.5 MJ / m² / day) in Kharga station and about (19 MJ / m² / day) in Kharga station. As a result of the apparent movement of the sun from the tropics during the summer to the equator during the spring, which leads to an increase in solar radiation during the spring months, where the amount of solar radiation at Kharga station is (27.5 MJ / m² / day) , while in Kharga station is (27.6 MJ / m² / day) (Ismael, H., 2015). The summer solar radiation doubles that record during the winter, where the amount of solar radiation at Kharga station about (29.7 MJ / m² / day) in summer. The sun apparent movement to the south during the autumn leads to decrease the amount of solar radiation of the Kharga oasis, it's about (22.3 MJ / m² / day).

The air temperature differs, chiefly in the summertime; when it may range from 7 °C at night, to 52 °C during the day. While the winter temperatures in Kharga oasis do not oscillate so wildly, they can be as low as 0 °C at night, and as high as 25 °C during the day. The absolute temperature is one of the most important indicators of the reality of the climatic conditions that characterize Kharga oasis. To clarify this further, Egypt's formal heat record is 50.3°C measured by British colonial officials at Kharga Oasis on June 9, 1961. Wherefore, Kharga oasis is part of the most hyper-arid place in the world. There is essentially no precipitation. Winds are predominant from the north. The temperature ranges from 5 °C to 26 °C in winter and from 26 °C to 45 °C in summer (Ismael, H., 2015).

Wind speed tends to be low in August, increases gradually from November to January, and reaches a peak from March to May causing dust storms famously known as "El-Khamsin". The annual mean value of relative humidity is 39.3%. It is very much lower at noon than at either morning or evening. The atmospheric precipitation as rainfall is extremely scarce and insignificant (~1 mm/yr).

Consequently, the category of extremely arid climate, with a category less than 0.05, represents about 41% of the total Oasis area. The dry climate category 0.05 to less than 0.2 covers about 21.7%. While, the semi-humid and humid climate categories represent about 18.6% of total area of the Oasis, according to value climate index (Table.8).

(Table.8) Climate type index according to geographical distribution in Kharga Oasis

| Category | Climate type | Indices | Area km ² | % |
|--------------|--------------|----------|----------------------|------|
| 1 | Hyper Arid | < 0.05 | 7827.5 | 41.6 |
| 2 | Arid | 0.05-0.2 | 4077.4 | 21.7 |
| 3 | Semi-Arid | 0.2-0.5 | 3406.5 | 18.1 |
| 4 | Semi-Humid | 0.5-0.65 | 1602.1 | 8.5 |
| 5 | Humid | > 0.65 | 1900.3 | 10.1 |
| Total | | | 18813.7 | 100 |

The interaction coefficient was applied to analyze the strength of the temperature relations with time. A linear trend was applied to find out the temperature trends from the period 1940 to 2018.

(Table. 9) Linear trends (in °C/decade) computed for annual and seasonal temperature in Kharga station (1940-2018). the associated 95% confidence intervals

| Time-scale | Linear trend (°C/decade) | 95% confidence intervals |
|--------------|--------------------------|--------------------------|
| Annual | 0.37 | (0.054/0.155) |
| DJF (Winter) | 0.47 | (0.083/0.174) |
| MAM (Spring) | 0.36 | (0.067/0.191) |
| JJA (Summer) | 0.49 | (0.086/0.189) |
| SON (Autumn) | 0.13 | (0.018/0.152) |

Annual temperature deviations computed from 1940 to 2018 demonstrate a definite rising trend of 0.35°C/decade, statistically significant at the 99% level (Table. 9). This is rational with the Kharga temperature increase characterized by (Domroes et al, 2005, Hossam Ismael, 2015, and Climatic Research Unit, University of East Anglia 2018) for the period 1940-2000. Moreover, seasonal temperature anomalies also display a distinct rise of 0.470 °C/decade for winter (DJF); 0.360 °C/decade for spring (MAM); 0.490 °C/decade for summer (JJA); and 0.130 °C/decade for autumn (SON), all statistically considerable at the 99% level (Table 9). The summer and the spring are the seasons with the greatest ranks of change while winter and autumn show lower trends.

Mostly, the soil temperatures in Kharga oasis have not been studied as much as other climate elements, such as air temperature, solar radiation and

rainfall, because the data are not vastly obtainable for spatial or temporal coverage (Budong Qian et al, 2011). For the current study, Kharga station provided daily soil temperature data at depths of 5, 10, 20, 50, 100, and 150 cm, beginning between 2006 until now. We had some missing data so we selected the mean annual soil temperature at depth of 10 cm between 2012 and 2018 from this station data set.

It appears however that Annual mean soil temperatures between 18 and 38 °C, and it has been clear from the analysis of (figure.6), that the soil temperature decreases in the margins of the Kharga Oasis, which represents the highest areas in the level, while the flat and low areas are affected by a large increase of temperature and high amount of evaporation.

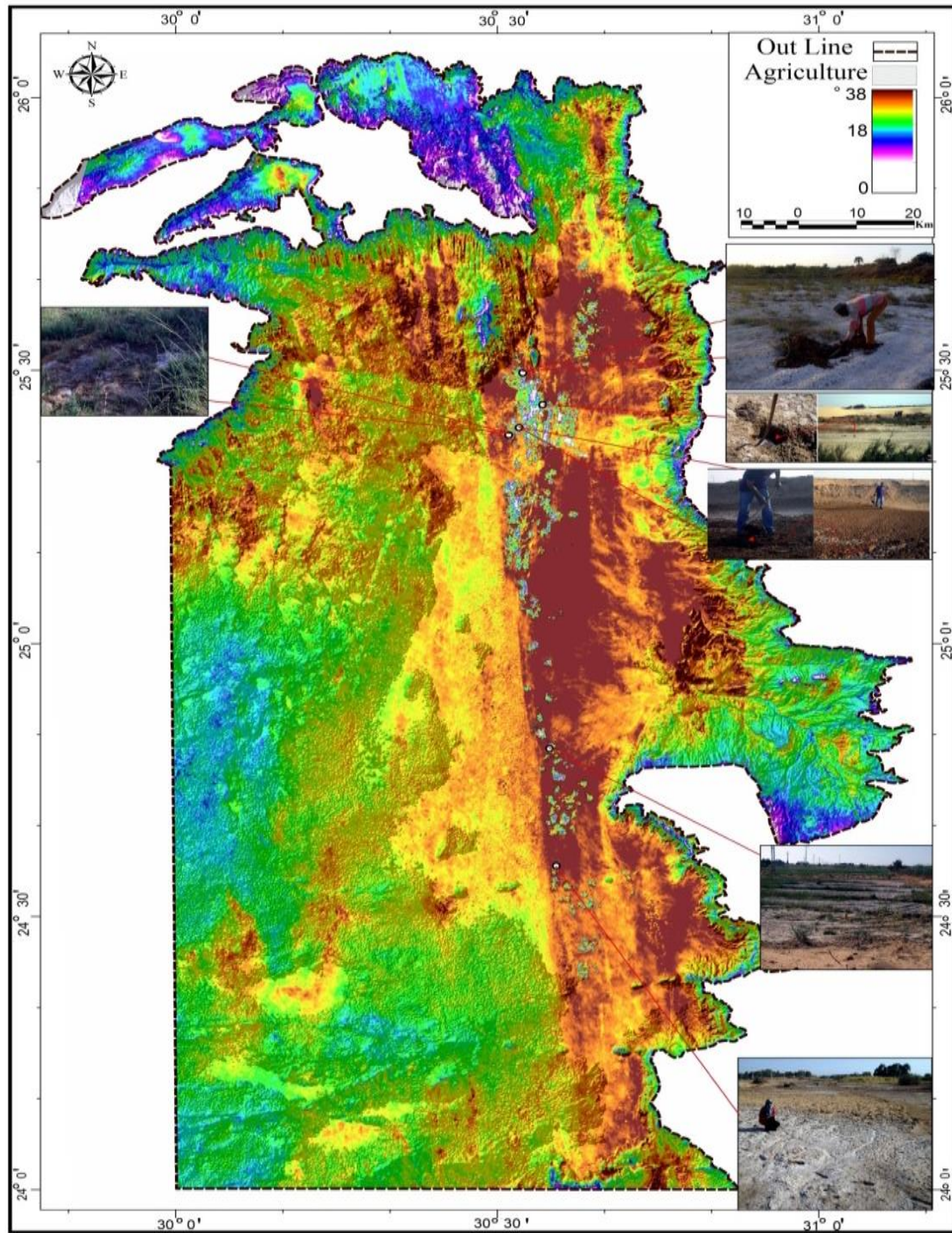


(Figure.6) The annual average soil temperature of Kharga station from 2010-2018

5-Conclusions:

The existence of Kharga Oasis in a hyper-arid desert is a direct reason for soil salinization due to the climate conditions and scarcity of water balance. Although groundwater is available, excessive discharge due to the expected development of the region could diminish water required to sustain agriculture and soil resources. Salinization in Kharga is attributed mainly to the nature of the Oasis, which is lower than the surrounding desert. The consequence of this is that the Oasis floor is close to the groundwater allowing evaporation of water and concentrations of salts at the soil surface leading to primary salinization.

Poor drainage, which results in water logging problems, also concentrates salts at the soil surface promoting secondary salinization. This study confirms that the available and free imagery can assist in monitoring the regional distribution of surface soil salinity. Detailed soil studies are recommended to characterize their physico-chemical characteristics and major salt type. Recognizing the system and motivating demands of mitigate the salinization in Kharga oasis could help develop appropriate administration of water sources, soils, and agricultural areas.

It was clear from the present study that remote sensing data is a powerful and effective tool in innovating of soil salinization maps. Where the study concluded that the best index used in extract soil salinity from Landsat-8 OLI satellite images is the first index S1, which is the Sqrt the second spectral band \times the fourth spectral band, where the value of the coefficient relation was 0.99, immediately followed by the eighth index, where the value of the coefficient of relation was 0.91.

Several important geographical factors caused the soil salinity problem in kharga oasis, the climate was the most significant factor, where the Kharga Oasis is located climatically in the dry, high-temperature and highly evaporative range, so the salts are concentrated. Among the geographical factors that cause soil salinity of Kharga Oasis is the anthropogenic influence, which comes second in the effect, where irrigation is spread by flooding the cultivated lands, and as a result of the topography of the lower Kharga Oasis, the salt-bearing water collects and evaporates, leaving concentrated salts in the soil, in addition to seepage saltwater from places Adjacent to the soil and agricultural land, in addition to following primitive irrigation patterns and useless agricultural policy.

About Eighty-five percent of bare and fallow soils in the Oasis have salinity values higher than 4dS/m. The impacts of this salinization are

manifested in soil and vegetation. It has been found that the area of extremely saline occupies an area of 6668 km² or about 35.5% of the total area of Kharga Oasis. Also, it was revealed through the study of the spatial distribution of soil salinity that the high salinity category is about 22.2%, and occupies 4733.7 km², and the moderate and low salinity categories include 24% and 15.3%, covers about 5462.6 km² and 2820 km² of Kharga Oasis respectively. The climate, anthropogenic factors and the low-level existence are the direct causes of soil salinization. Quantification of the extent of soil salinity is crucial for proper management of the region.

The old irrigation regimes in Kharga oasis are one essential reason for human-induced soil salinization. The lack of a well-developed drainage system had led to an enhanced water table and by time water had recharged the deepest area in the Oasis to serve as a big artificial lake, Lake El-Sheikh. Uncontrolled drainage has still caused significant water-logged areas. Barren and fallow soils of Kharga are generally saline, where their EC values are more than 4 dS/m.

Ultimately, it has been concluded that the soil salinization hazard was spreading

due to the climate conditions, widespread irrigation system, and internal drainage. It has also been demonstrated that the slope degree of the land becomes a significant impact on the salinization and had an expulsive relationship between them. Based on the results of the study, it is recommended that extending the use of remote sensing data, especially high-spatial and spectral resolution ones, in studying soil properties, it is considered effective and powerful techniques and tools in studying and monitoring soil salinity problem.

Conflict of Interests

The authors declare that there is no conflict of interests concerning the publication of this study.

References:

1. Abbas, A., Khan, S., Hussain, N., Hanjra, M.A., Akbar, S., 2013. Characterizing soil salinity in irrigated agriculture using a remote sensing approach. *Phys. Chem. Earth Parts A/B/C* 55–57, 43–52.
2. Abbas, A., Khan, S., 2007. Using remote sensing technology for appraisal of irrigated soil salinity. pp. 2632–2638.
3. Abdul-Qadir, A.M.H., Benni, T.J., 2010. Monitoring and evaluation of soil salinity in term of spectral response using Landsat images and GIS in Mesopotamian plain/Iraq. *J. Iraqi Desert Stud.* 2, 19–32.
4. Abdelgadir, A. Rubab A., 2019. Mapping soil salinity in arid and semi-arid regions using Landsat 8 OLI satellite data. *Remote Sensing Applications: Society and Environment* 13 (2019) 415–425
5. Allbed, A., Kumar, L., Sinha, P., 2014. Mapping and modelling spatial variation in soil salinity in the Al Hassa Oasis based on remote sensing indicators and regression techniques. *Remote Sens.* 6, 1137–1157.
6. Allbed, A., Kumar, L., Aldakheel, Y.Y., 2014. Assessing soil salinity using soil salinity and vegetation indices derived from IKONOS high-spatial resolution imagery: applications in a date palm dominated region. *Geoderma* 230, 1–8.
7. Amal Allbed, Lalit Kumar & Priyakant Sinha (2017): Soil salinity and vegetation cover change detection from multi-temporal remotely sensed imagery in Al Hassa Oasis in Saudi Arabia, *Geocarto International*, DOI: 10.1080/10106049.2017.1303090
8. Al-Khaier, F., 2003. Soil salinity detection using satellite remote sensing. *Geo-Inf. Sci. Earth Obs. Int. Inst. Geo-Inf. Sci. Earth Obs.* 70.
9. Alizade Govarchin Ghale, Y., Baykara, M., & Unal, A. 2017. Analysis of decadal land cover changes and salinization in Urmia Lake Basin using remote sensing techniques. *Natural Hazards and Earth System Sciences Discussions*, 1–15. doi:10.5194/nhess-2017-212
10. Arnous, M.O., El-Rayes, A.E. & Green, D.R. (2015). Hydrosalinity and environmental land degradation assessment of the East Nile Delta region. *Egypt. J. Coast. Conserv.*, 19, 491–513.
11. Arnous, M.O. & Green, D.R. (2015). Monitoring and assessing waterlogged and salt-affected areas in the Eastern Nile Delta region, Egypt, using remotely sensed multi-temporal data and GIS. *J. Coast. Conserv.*, 19, 369–391.

12. Bannari, A., Guedon, A.M., El-Harti, A., Cherkaoui, F.Z., El-Ghmari, A., 2008. Characterization of slight and moderate saline and sodic soils in irrigated agricultural land using simulated data of ALI (EO-1) sensor. *Commun. Soil Sci. Plant Anal.* 39, 2795–2811. <https://doi.org/10.1080/00103620802432717>.
13. Bing Guo, Wenqian Zang, Wei Luo, Ye Wen, Fei Yang, Baomin Han, Yewen Fan, Xi Chen, Zhen Qi, Zhen Wang, Shuting Chen & Xiao Yang (2020) Detection model of soil salinization information in the Yellow River Delta based on feature space models with typical surface parameters derived from Landsat8 OLI image, *Geomatics, Natural Hazards and Risk*, 11:1, 288-300, DOI: 10.1080/19475705.2020.1721573
14. Bai, Z.G., Dent, D.L., Olsson, L., Schaepman, M.E., 2008. Proxy global assessment of land degradation. *Soil Use Manage.* 24 (3), 223–234.
15. Budong Qian., Edward G. Gregorich, Sam Gameda., David W. Hopkins., Xiaolan L. Wang, 2011. Observed soil temperature trends associated with climate change in Canada, *JOURNAL OF GEOPHYSICAL RESEARCH*, VOL. 116, D 02106, doi:10.1029/2010JD015012, 2011
16. Clarke, C.J., George, R.J., Bell, R.W., Hatton, T.J., 2002. Dryland salinity in south-western Australia: its origins, remedies, and future research directions. *Soil Res.* 40 (1), 93–113.
17. Chhabra, R. 2014. Classification of Salt-Affected Soils. *Arid Land Research and Management*, 19: 61-79.
18. Casterad, A. 2018. Assessment of soil salinity during the first years of transition from flood to sprinkler irrigation. *Sensors.*, 18, 616.
19. Chavez PS. 1996. Image-based atmospheric correction – revised and improved. *Photogramm Eng Remote Sens.* 62:1025–1036.
20. Das, S., Choudhury, M.R. & Das, S. 2016. Earth observation and geospatial techniques for soil salinity and land capability Assessment over Sundarban Bay of Bengal Coast, India. *Geodesy and Cartography.* 65, 163–192.
21. Dehni, A., Lounis, M., 2012. Remote sensing techniques for salt affected soil mapping: application to the Oran region of Algeria. *Procedia Eng.* 33, 188–198.

22. Dellavalle NB. 1992. Determination of soil-paste pH and conductivity of saturation extract. In: Dellavalle NB, editor. Handbook on reference methods for soil analysis. Athens: Soil and Plant Analysis Council, Inc.; pp. 40–43.
23. Ding, J., Yu, D., 2014. Monitoring and evaluating spatial variability of soil salinity in dry and wet seasons in the Werigan–Kuqa Oasis, China, using remote sensing and electromagnetic induction instruments. *Geoderma* 235–236, 316–322.
24. Douaoui, A.E.K., Nicolas, H., Walter, C., 2006. Detecting salinity hazards within a semiarid context by means of combining soil and remote-sensing data. *Geoderma* 134, 217–230.
25. Dehni, A., Lounis, M., 2012. Remote sensing techniques for salt affected soil mapping: application to the Oran region of Algeria. *Procedia Eng.* 33, 188–198.
26. Dehaan, R. L., & Taylor, G. R. (2002). Field-derived spectra of salinized soils and vegetation as indicators of irrigation-induced soil salinization. *Remote Sensing Environment*, 80(3), 406–417. [https://doi.org/10.1016/S0034-4257\(01\)00321-2](https://doi.org/10.1016/S0034-4257(01)00321-2).
27. Didi, S., Housni, F. E., Najine, A., Wafik, A., Aadraoui, M., Hafiane, F. Z., et al. (2017). Mapping and characterization of agricultural systems from time series of Normalized Difference Vegetation Index (NDVI) in the northeast area of Tadla, Morocco. *Natural Resources*, 8(1), 24–30. <https://doi.org/10.4236/nr.2017.81002>.
28. Domroes, M., and El-Tantawi, A., 2005: recent temporal and spatial temperature changes in EGYPT, *INTERNATIONAL JOURNAL OF CLIMATOLOGY*, Int. J. Climatol. 25: 51–63.
29. Ebraheem AM, Riad S, Wycisk P, Sefelnasr AM. 2004. A local-scale groundwater flow model for groundwater resources management in Dakhla Oasis, SW Egypt. *Hydrogeol J.* 12:714–722.
30. El, A., Lhissou, R., Chokmani, K., Ouzemou, J., Hassouna, M., Mostafa, E. & El, A. 2016. Spatiotemporal monitoring of soil salinization in irrigated Tadla Plain (Morocco) using satellite spectral indices. *Int. J. Appl. Earth Obs. Geoinf.*, 50, 64–73.
31. El-Battay, A., Bannari, A., Hameid, N.A., Abahussain, A.A., 2017. Comparative study among different semi-empirical models for soil salinity prediction in an arid environment using OLI Landsat-8 data. *Adv. Remote Sens.* 6, 23–39. <https://doi.org/10.4236/ars.2017.61002>.

- 32.Eldeiry, A.A., Garcia, L.A., 2008. Detecting soil salinity in alfalfa fields using spatial modeling and remote sensing. *Soil Sci. Soc. Am. J.* 72, 201–211.
- 33.Eldeiry, A.A., Garcia, L.A., 2010. Comparison of ordinary kriging, regression kriging, and cokriging techniques to estimate soil salinity using LANDSAT images. *J. Irrig. Drain. Eng.* 136 (6), 355–364.
- 34.Elhag, M., 2016. Evaluation of different soil salinity mapping using remote sensing techniques in arid ecosystems, Saudi Arabia. *J. Sens.* 2016.
- 35.Elhag, M., 2016. Evaluation of different soil salinity mapping using remote sensing techniques in arid ecosystems, Saudi Arabia. *J. Sens.* 2016.
- 36.Evans, G., Schmidt, V., Bush, P., Nelson, H., 1969. Stratigraphy and geologic history of the sabkha Abu Dhabi, Persian Gulf, *Sedimentology*. *Sedimentology* 12, 145.
- 37.Elnaggar, A.A., Noller, J.S., 2009. Application of remote-sensing data and decision-tree analysis to mapping salt-affected soils over large areas. *RemoteSens.* 2 (1), 151–165.
- 38.Fan, X., Liu, Y., Tao, J., Weng, Y., 2015. Soil salinity retrieval from advanced multi-spectral sensor with partial least square regression. *Remote Sens.* 7 (1), 488–511.
- 39.Fan, X., Weng, Y., Tao, J., 2016. [Towards decadal soil salinity mapping using Landsat time series data. *Int. J. Appl. Earth Obs. Geoinf.* 52, 32–41.](#)
- 40.Fang, H., Liu, G., Kearney, M., 2005. Georelational analysis of soil type, soil salt content, landform, and land use in the Yellow River Delta, China. *Environ.Manage.* 35 (1), 72–83.
- 41.Farifteh, J., Farshad, A., George, R.J., 2006. Assessing salt-affected soils using remote sensing, solute modelling, and geophysics. *Geoderma* 130 (3), 191–206.
- 42.Ghadiry M, Shalaby A, Koch B. 2012. A new GIS-based model for automated extraction of sand dune encroachment case study: Dakhla Oases, western desert of Egypt. *Egypt J Remote Sens Space Sci.* 15:53–65.
- 43.Gorji, T. 2016. Monitoring Soil Salinity VIA Remote Sensing Technology under data scarce conditions: A Case Study from Turkey, M.Sc. Thesis, Department of Environmental Engineering, Istanbul

- Technical University, Graduate School of Science Engineering and Technology.
44. Gorji, T., Sertel, E., Tanik, A., 2017. [Monitoring soil salinity via remote sensing technology under data scarce conditions: A case study from Turkey. *Ecol. Indic.* 74, 384–391.](#)
45. Gorji et al. 2019. Remote sensing approaches and mapping methods for monitoring soil salinity under different climate regimes, *International Journal of Environment and Geoinformatics (IJECEO)*, 6(1): 33-49. DOI: 10.30897/ijegeo.500452.
46. Goossenes, R. and Vanranst, E. 1996. The Use of Remote Sensing and GIS to Detect Gypsiferous Soils in the Ismailia Province (Egypt). Proceedings of the International Symposium on Soils with Gypsum. Lieida, 15-21, September, 1996. Catalonia, Spain.
47. Hereher, M., M. Salem, and H. Abdel Hamid. (2010): Change Detection of Salt- Affected Soils at the Coastal Zone of the Nile Delta Using Remote Sensing. *Egypt J Soil Sciences*, 50: 111-123.
48. Hereher M. 2014. Assessment of sand drifts potential along the Nile Valley and Delta using climatic and satellite data. *Appl Geogr.* 55:39–47.
49. Ismael, H., 2015. Evaluation of present –day climate induced desertification in El-Dakhla Oasis, western desert of Egypt, based on integration of MEDALUS method, GIS and RS. *De GRUYETER, Present Environment and Sustainable Development. Volume 9, Issue 2, October 2015, Pages 47–72.* DOI: [10.1515/pesd-2015-0024](#).
50. Ismael, H., 2016. Monitoring Drought Trends Induced Climate Variability over Egypt Using MODIS NDVI Satellite Data and Drought Indices. *Bulletin de la Société de Géographie d’Egypte*, 89(1), 91-121. doi: 10.21608/bsge.2016.90342
51. Ivushkin, K., Bartholomeus, H., Bregt, A.K., Pulatov, A., Kempen, B., de Sousa, L., 2019. [Global mapping of soil salinity change. *Remote Sens. Environ.* 231, 111260.](#)
52. Kallel, A.; Ksibi, M.; Dhia, H.B.; Khélifi, N. Erratum to: Recent Advances in Environmental Science from the Euro-Mediterranean and Surrounding Regions. Euro-mediterranean Conference for Environmental Integration. Springer International Publishing: Cham, Switzerland, 2017.

53. Khan, N.M., Rastoskuev, V.V., Shalina, E.V., Sato, Y., 2001. Mapping salt-affected soils using remote sensing indicators a simple approach with the use of GIS IDRISI. In: Proceedings of the 22nd Asian Conference on Remote Sensing vol. 5, pp. 9.
54. Khan, N.M., Rastoskuev, V.V., Sato, Y., Shiozawa, S., 2005. Assessment of hydrosaline land degradation by using a simple approach of remote sensing indicators. *Agric. Water Manag.* 77, 96–109.
55. Kumar, N., Singh, S.K., Pandey, H.K., 2018. *Appl. Geomath.* <https://doi.org/10.1007/s12518-018-0218-2>.
56. Ma, L., Yang, S., Simayi, Z., Gu, Q., Yang, X., Ding, J., 2018. Modeling variations in soil salinity in the oasis of Junggar Basin, China. *Land Degrad. Dev.* 29, 551–562.
57. Masoud, A. A. and K. Koike 2006. Arid land salinization detected by remotely-sensed landcover changes: A case study in the Siwa region, NW Egypt. *Journal of Arid Environments* 66: 151–167.
58. Masoud, A.A., 2014. Predicting salt abundance in slightly saline soils from Landsat ETM+ imagery using Spectral Mixture Analysis and soil spectrometry. *Geoderma* 217–218, 45–56.
59. Masoud, A.A., Koike, K., Atwia, M.G., El-Horiny, M.M., Gemail, K.S., 2019. Mapping soil salinity using spectral mixture analysis of landsat 8 OLI images to identify factors influencing salinization in an arid region. *Int. J. Appl. Earth Obs. Geoinf.* 83, 101944.
60. Metternicht G. I., J. A. Zinck. 2003. Remote sensing of soil salinity: potential and constraints. *Remote Sensing of Environment*, 85: 1-20.
61. Mohamed E. Hereher & Hossam Ismael (2016): The application of remote sensing data to diagnose soil degradation in the Dakhla Oasis – Western Desert, Egypt, Geocarto International, DOI: 10.1080/10106049.2015.1059901
62. Metternicht, G., Zinck, J.A., 1997. Spatial discrimination of salt-and sodium-affected soil surfaces. *Int. J. Remote Sens.* 18, 2571–2586.
63. Metternicht, G.I., Zinck, J.A., 2003. Remote sensing of soil salinity: potentials and constraints. *Remote Sens. Environ.* 85, 1–20.
64. Mostafa El Gamal, 2016. Water in Egypt, HafenCity Universität Hamburg, Resource Efficiency in Architecture and Planning (REAP), Urban Water Cycles, summer semester 2012.

65. Mousavi et al. 2017. Digital Mapping of Topsoil Salinity Using Remote Sensing Indices in Agh-Ghala Plain, Iran, 5 (2), PP. 1771-1786.
66. M.M. Jordan; J. Navarro-Pedren; E. Garcí'a-Sa´nchez; J. Mateu and P. Juan, Spatial dynamics of soil salinity under arid and semi-arid conditions: geological and environmental implications, 2004, Environmental Geology, 45:448–456, DOI 10.1007/s00254-003-0894
67. Lhissou ,R. et al 2014. Mapping soil salinity in irrigated land using optical remote sensing data, Canada Eurasian Soil Science Societies (CESSS). ,pp.81-88.
68. Liping Yang, Xingmin Meng & Xiaoqiang Zhang, 2011 SRTM DEM and its application advances, International Journal of Remote Sensing, 32:14, 3875-3896, DOI: 10.1080/01431161003786016
69. Poenaru, V., Badea, A., Cimpeanu, S. Mihai, & Irimescu, A. (2015). Multi-temporal Multi-spectral and Radar Remote Sensing for Agricultural Monitoring in the Braila Plain. *Agriculture and Agricultural Science Procedia*, 6, 506-516. doi: [10.1016/j.aaspro.2015.08.134](https://doi.org/10.1016/j.aaspro.2015.08.134)
70. Rattan Lal, Bal Ram Singh, Dismas L. Mwaseba, David Kraybill, David O. Hansen, Lars Olav Eik, 2014. Sustainable Intensification to Advance Food Security and Enhance Climate Resilience in Africa. Springer, Cham., Nature - 665 p.
71. Rao, B.R.M., Dwivedi, R.S., Venkataratnam, L., Ravishankar, T., Thammappa, S.S., Bhargawa, G.P., Singh, A.N., 1991. Mapping the magnitude of sodicity in part of the Indo-Gangetic plains of Uttar Pradesh, Northern India using Landsat-TM data. *Int. J. Remote Sens.* 12, 419–425.
72. Rao B, T. Sankar, R. Dwivedi, S. S. Thammappa, L. Venkataratnam, R. C. Sharma, S N. Das. 1995. Spectral behavior of salt-affected soils. *International Journal of Remote Sensing*, 16: 2125-2136.
73. Rajesh Kumar and Amar Jyoti Das, 2014. Climate Change and its Impact on Land Degradation: Imperative Need to Focus, *J Climatol Weather Forecasting* 2014, 2:1 DOI: 10.4172/2332-2594.1000108
74. Salahddine Didi., Fatima Ezzahra Housni., Humberto Bracamontes., Abdessamad Najine., 2019. Mapping of Soil Salinity Using the Landsat 8 Image and Direct Field Measurements: A Case

- Study of the Tadla Plain, Morocco. *Journal of the Indian Society of Remote Sensing* (July 2019) 47(7):1235–1243
75. Shahid S.A., Zaman M., Heng L. (2018) Soil Salinity: Historical Perspectives and a World Overview of the Problem. In: *Guideline for Salinity Assessment, Mitigation and Adaptation Using Nuclear and Related Techniques*. Springer, Cham.
76. Srivastava, A., Tripathi, N.K., Gokhale, K., 1997. Mapping groundwater salinity using IRS- 1B LISS II data and GIS techniques. *Int. J. Remote Sens.* 18, 2853–2862.
77. Setia, R., Lewis, M., Marschner, P., Raja Segaran, R., Summers, D. & Chittleborough, D. (2013). Severity of salinity accurately detected and classified on a paddock scale with high resolution multispectral satellite imagery. *Land Deg. and Development.*, 24, 375–384.
78. Soltan, M. (1999): Evaluation of groundwater quality in Kharga Oasis (Egyptian Western Desert). *Environmental Monitoring and Assessment* 57: 157–168.
79. Shrestha, D.P., Soliman, A.S., Farshad, A., and Yadav, R.D. 2005b. Salinity mapping using geopedologic and soil line approach. In *Proceedings of the 26th Asian Conference of Remote Sensing*, Hanoi, Vietnam.
80. Saghafi, M. 2017. Application of remote sensing indices for mapping salt-affected areas by using field data methods. *International Journal of Advanced and Applied Sciences*, 4, 181–187.
81. Taha Gorji., Aylin Yıldırım., Elif Sertel., Aysegül Tanık., 2019. Remote sensing approaches and mapping methods for monitoring soil salinity under different climate regimes, *International Journal of Environment and Geoinformatics* 6(1): 33-49.
82. Tran, T.V., Tran, D.X., Myint, S.W., Huang, C., Pham, H.V., Luu, T.H., 2019. [Examining spatiotemporal salinity dynamics in the Mekong River Delta using Landsat time series imagery and a spatial regression approach. *Sci. Total Environ.* 687, 1087–1097.](#)
83. Vermeulen, D. & Niekerk, A.V. 2017. Geoderma Machine learning performance for predicting soil salinity using different combinations of geomorphometric covariates. *Geoderma*, 299, 1–12
84. Vicente-Serrano SM, Lopez-Moreno J-I, Beguería S, Lorenzo-Lacruz J, Sanchez-Lorenzo A, García-Ruiz JM, Azorin-Molina C, Revuelto J, Trigo R, Coelho F, Espejo F. 2014. Evidence of increasing drought

- severity caused by temperature rise in southern Europe. Environ. Res. Lett. 9: 044001, doi: 10.1088/1748-9326/9/4/044001.
85. Weng, Y.L., Gong, P., Zhu, Z.L., 2010. A spectral index for estimating soil salinity in the Yellow River Delta region of China using EO-1 Hyperion data. *Pedosphere* 20 (3), 378–388.
86. Wulder, M.A., Loveland, T.R., Roy, D.P., Crawford, C.J., Masek, J.G., Woodcock, C.E., et al., 2019. [Current status of Landsat program, science, and applications](#). *Remote Sens. Environ.* 225, 127–147.
87. Yahiaoui, I., Douaoui, A., Zhang, Q. & Ziane, A. 2015. Soil salinity prediction in the Lower Cheliff plain (Algeria) based on remote sensing and topographic feature analysis. *J. Arid Land*, 7, 794–805.
89. Ye. I. Pankova and M. V. Konyushkova., 2013. Effect of Global Warming on Soil Salinity of the Arid Regions, *Russian Agricultural Sciences*, 2013, Vol. 39, No. 5–6, pp. 464–467.
90. Youssef, A.M., Pradhan, B., Sabtan, A.A., El-Harbi, H.M., 2012. Coupling of remote sensing data aided with field investigations for geological hazards assessment in Jazan area, Kingdom of Saudi Arabia. *Environ. Earth Sci.* 65, 119–130.
91. Zhang, L. "Analysis of geo-hazards caused by climate changes", *Landslides and Engineered Slopes From the Past to the Future Proceedings of the 10th International Symposium on Landslides and Engineered Slopes 30 June - 4 July 2008 Xi an China, 2008.*

The effect of prevailing climatic conditions on detecting and monitoring soil Salinity of Kharga Oasis based on Landsat 8 OLI satellite and climate time series

Hossam Ismael

Assistant Professor, Geography
Department, Faculty of Arts,
New Valley University, Egypt
hosam.ismael@artnv.au.edu.eg

Waleed Abbas

Lecturer, Geography department,
Faculty of Arts, Ain Shams
University, Egypt
walid.abbas@art.asu.edu.eg

Sharbat Bashandi

Lecturer, Geography department,
Faculty of Arts, Cairo University, Egypt
sharabathamdy@yahoo.com

Abstract

occupies an area of 6668 km² or about 35.5% of the total area of Kharga Oasis. Also, it was revealed through the study of the spatial distribution of soil salinity that the high salinity category is about 22.2%, and occupies 4733.7 km², and the moderate and low salinity categories include 24% and 15.3%, covers about 5462.6 km² and 2820 km² of Kharga Oasis, respectively. The climate, anthropogenic factors, and the low-level existence are the direct causes of soil salinization in Kharga Oasis.

salinization, and as a result, it is becoming a serious economic and environmental concern in New Valley governorate. Detecting and monitoring soil salinization in Kharga Oasis is accordingly important to support decision-making procedures for lessening adverse effects of land degradation due to the salinization, especially to kharga oasis, as one of the promising regions for agricultural development in Egypt. Clearly, satellite data-based technologies supply cost-efficient, rapid, qualitative spatial data on soil salinity. Kharga Oasis in the Western Desert of Egypt is experiencing pronounced prevailing climatic condition induced geo-hazards such as soil salinization. The present study aimed to study the effect of prevailing climatic conditions on detecting and monitoring soil salinization of Kharga Oasis. To achieve the study aims, the present study used operating remote sensing and GIS techniques, soil sampling synchronized with a satellite image from the Landsat-8 Operational Land Imager (OLI) Level 1T product during July 2018 have been analyzed by regression correlation analysis. The present study was based not only on raw climate data and satellite images but also on field investigations of Kharga Oasis. About Eighty-five percent of bare and fallow soils in the Oasis have salinity values more than 4dS/m. The impacts of this salinization are illustrated in soil and vegetation. It has been found that the area of extremely soil saline

Keywords: Climate conditions, evaporation, salinization, remote sensing, Kharga.